

The Simulation of Diaphragm Deflection Actuated by Shear Mode Piezoelectric Actuator in Microdroplet Ejector

C. H. Cheng¹, S. C. Chen²

Abstract: A shear mode piezoelectric actuator is applied to deflect the diaphragm of pressure chamber in the droplet ejector or inkjet printhead. The deflection of the bulge-diaphragm and resulting swept volume is analyzed by analytical and numerical method. With free-body treatment of the model, the analytical exact solutions for the two free bodies of bulge-diaphragm and piezoelectric beam were obtained. Also, the numerical solution by ANSYS is obtained to verify the analytical result. Besides, the whole-model solution coupling the bulge-diaphragm and piezoelectric beam together was obtained by ANSYS to compare with the result of free-body analysis. In order to estimate the maximum actuating force and deflection of the shear mode piezoelectric actuator, the *piezoelectric characteristic curve* is obtained in the free-body analysis, which presents the decreasing tendency of the central deflection with the increase of anti-deflection (or reaction) force under certain actuating voltage. Also, the *diaphragm characteristic curve* is obtained showing the central deflection in proportion to the action force. By combining both kinds of curves, the actuated central deflection of the bulge-diaphragm can be obtained under certain actuating voltage. Finally, both linear relations including diaphragm central deflection in proportion to actuating voltage and volume displacement in proportion to diaphragm central deflection are obtained.

keyword: piezoelectric actuator, shear mode, droplet ejector, simulation, inkjet printing.

1 Introduction

In the past decade, the most valuable application of microdroplet ejection technology is the inkjet printing on paper. Recently, many emerging applications make microdroplet ejection technology more and more important,

including direct writing of organic polymer solution for lighting device of flat panel displays [Yang et al. (2000), Hebner et al. (1998), Edwards et al. (2001)], photoresist on substrate [Percin et al. (2003)], solder bumps for flip chip electrical packaging [Haynes et al. (1999)] or solar cell metallization [Teng et al. (1998)], and biomedical and chemical sample handling [Luginbuhl (1999)]. There are mostly two kinds of actuation principle for droplet ejection technology, which are thermal bubble actuation [Keefe et al. (1994)] and piezoelectric actuation [Sakai et al. (1993), Zhang (2004)]. The piezoelectric actuation technique is favored if the ejecting fluid has the need to avoid thermal load (e.g. organic polymer solution). The droplet ejection by piezoelectric actuation was invented by Sweet [Sweet (1971)]. Based on the piezoelectric ceramics deformation mode, the piezoelectric actuated inkjet technology is divided into four main types including bend mode, push mode, squeeze mode and shear mode. Except for the shear mode, the polarization of piezoelectric actuator is parallel to external electrical field. However, in shear mode design, the piezoelectric actuator is poled along the direction perpendicular to applied electrical field. Fig.1 shows the schematic drawings of the four types of piezoelectric actuating modes for comparisons in inkjet technology. All actuating modes are designed in order for the same function of causing the volume change of pressure chamber or flow channel and ejecting droplet from orifice. For bend mode shown as Fig.1(a), the diaphragm attached with piezoelectric plate is deflected inwardly into the pressure chamber due to the extension difference between two layers. For push mode shown as Fig.1(b), the piezoelectric rod push the diaphragm by its extension effect. For squeeze mode shown as Fig.1(c), the radially poled piezoelectric tube provided with electrodes on its inner and outer surface is treated as pressure chamber and its squeeze effect makes droplet ejection possible. The fourth deformation type by shear mode actuator is known for Xaar-type inkjet head designed from Xaar

¹ DA-YEH University, ChangHua, Taiwan

² National Changhua University of Education, ChangHua, Taiwan

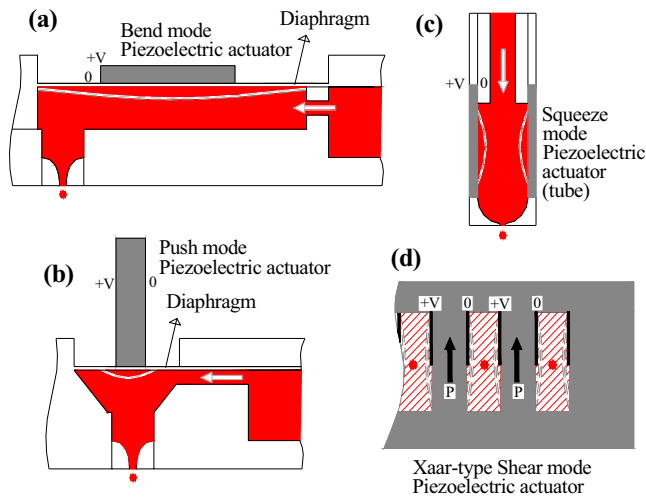


Figure 1 : Schematic of four piezoelectric ceramics deformation mode used in ejector technology

company [Brumahl et al. (2002)]. The poled piezoelectric plate is micromachined to form flow channel with the channel walls possessing polarization along wall standing direction. External electrical field applied along wall thickness direction is perpendicular to poled direction and causes shear deformation of channel wall and the resulting volume change of channel, showing in Fig.1(d). In this study, we propose a novel design of shear mode piezoelectric actuating module different from Xaar-type actuator for droplet ejector or inkjet printer. The module consists of a shear mode PZT actuator and vibration plate with the feature of bulge-diaphragm shown in Fig.2. The bulge-diaphragm means the structure including a diaphragm and two different-sized bulges piled up on the diaphragm. The shear mode PZT actuator is glued on and suspended between the top bulge and the surface of vibration plate, and through the bulges the diaphragm is deflected. Thus, the resulting sudden decrease of chamber volume cause droplet to be expelled from the orifice. Because the volume displacement of chamber plays a key role of droplet ejection, the study aims at the analytical and numerical solution for the deflection of the bulge-diaphragm and the resulting volume displacement.

2 Design and analysis

The purpose of the present paper is to propose a novel design of the shear mode piezoelectric actuating module for droplet ejector or inkjet printer. The bulge-diaphragm is

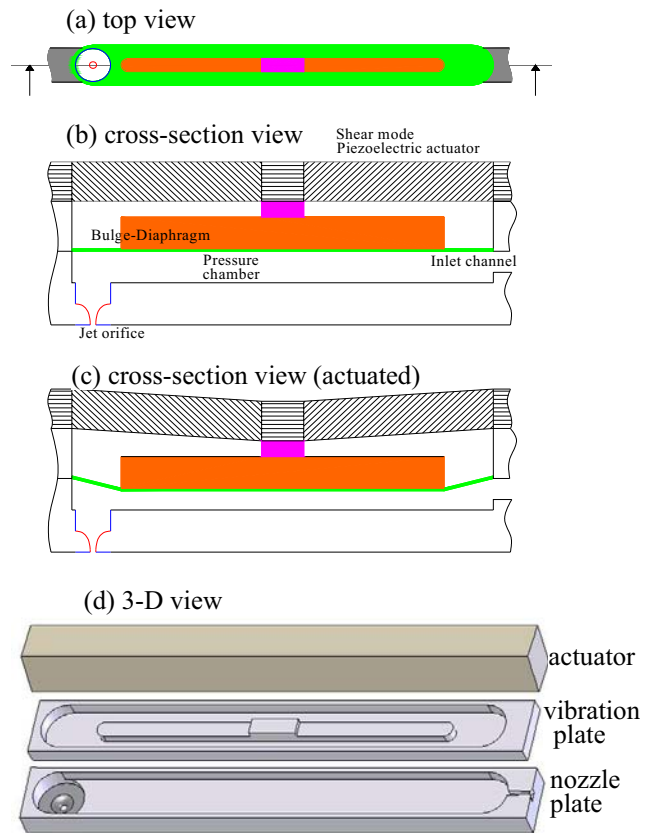


Figure 2 : Schematic of microdroplet ejector actuated by novel shear mode actuating module

deflected through the rigid bulges by piezoelectric actuator. Its deformation including out-of-plane displacement and swept volume is calculated by both analytical and numerical method. Taking piezoelectric actuator and bulge-diaphragm as a free body and introducing action/reaction force at interface, each deflection as a function of action or reaction force was obtained in analytical form or ANSYS numerical results. Since the reaction force restrains the deflection of the actuator, a curve named *piezoelectric characteristic curve* shows a decreasing tendency of the central deflection with the increase of reaction force. By the curve, the maximum output force and deflection of actuator can be estimated. And, the other relation of the bulge-diaphragm represented by *diaphragm characteristic curve* show the increasing tendency of the central deflection with the increase of action force. A detail description about design and analysis is presented in following sections. Two kind of model treatment was used to solve the problem including free-body and whole-

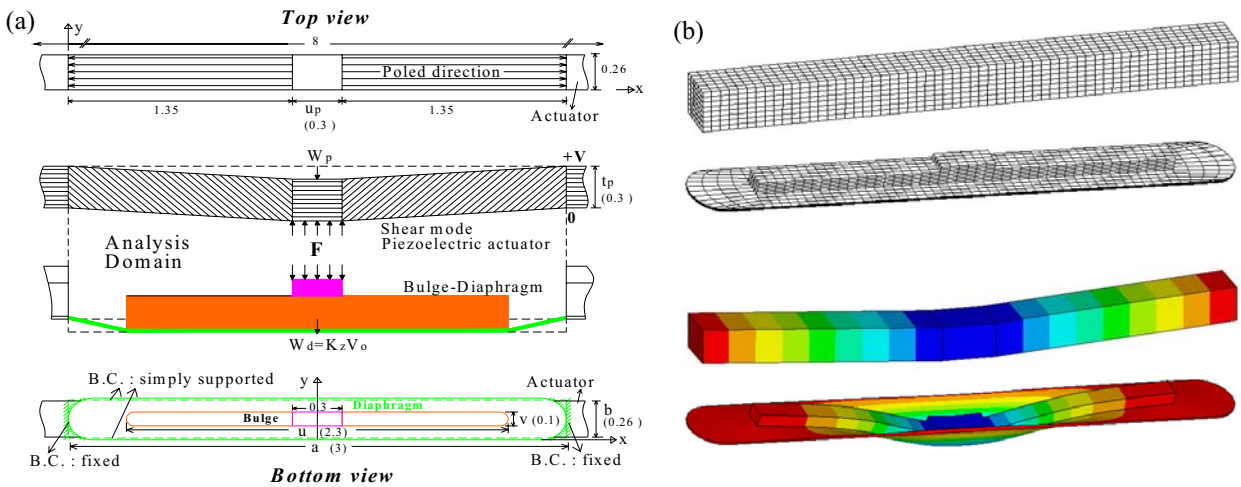


Figure 3 : Free-body diagram in analytical or numerical analysis (dimension in mm)

Table 1 : Mechanical properties for numerical and analytical solution

PZT5H								
Elastic stiffness (GPa)					Piezoelectric parameters ($e_{mn}, \text{C/m}^2$) ($d_{mn}, 10^{-12} \text{m/V}$)			
c_{11}^E	c_{12}^E	c_{13}^E	c_{33}^E	c_{44}^E	$e_{31}(d_{31})$	$e_{33}(d_{33})$	$e_{15}(d_{15})$	
126	79.5	84.1	117	23	-6.5(-274)	23.3(593)	17.7(741)	
Ni								
Elastic Modulus, E (GPa)			Density, ρ (Kg/m ³)			Poison ratio, ν		
210			8800			0.31		

model treatment. Both analytical and numerical method are used in free-body solution while the whole-model solution just obtained by numerical method.

As shown in Fig.2 and Fig.3, the shear mode piezoelectric actuator with beam shape processed by PZT5H piezoceramics has the dimensions of $8 \times 0.26 \times 0.3 \text{mm}$. And in top view it possesses two $0.26 \times 1.35 \text{mm}$ poled zones separated by a middle non-poled zone with dimension of $0.26 \times 0.3 \text{mm}$. Both poled zones are symmetrically and oppositely poled in lateral or length direction parallel to the plane of the plate. So, five zones were defined including the middle and the two outer non-poled zones and the two poled zones with symmetrically opposite poled directions. The vibration plate with the feature of two different sized bulges piled on the diaphragm is manufactured by electroforming nickel process. The thickness of bigger bottom bulge, say $60 \mu\text{m}$, is larger than the $30 \mu\text{m}$ thickness of the smaller top bulge. This design is considered to be capable of improving the vol-

ume displacement. The piezoelectric actuator is glued on and suspended between the top bulge and the surface of vibration plate. The applied electric field perpendicular to poled direction leads to shear effect, so that top bulge is pushed to deflect the diaphragm causing volume change of the pressure chamber.

To analyze the actuating force of the piezoelectric shear effect, as the analysis domain shown in Fig.3, we took two free bodies, piezoelectric beam and bulge-diaphragm, by separating actuating module at the bonding interface and introducing equal action and reaction force to respective separated interface. Both numerical, by ANSYS, and analytical solutions for deflection of each free body were analyzed at equilibrium static state. And, all mechanical properties of both PZT5H piezoceramics and nickel for analytical or numerical solution were listed in Table1.

For the free body of piezoelectric beam, the *piezoelectric characteristic curve* which shows the central deflec-

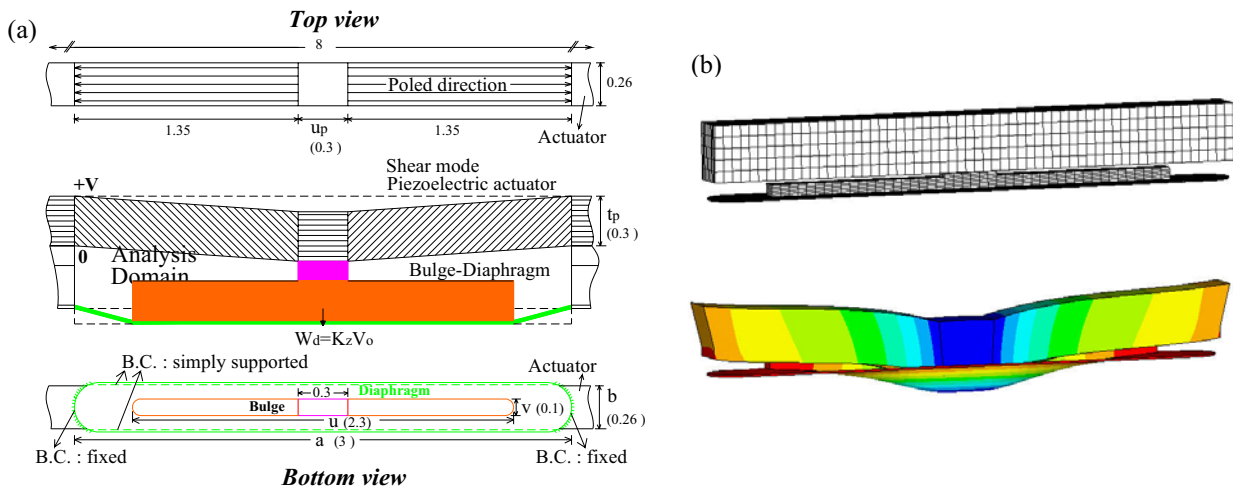


Figure 4 : Whole-model diagram of numerical analysis (dimension in mm)

tion decreasing with anti-deflection force (i.e. reaction force in free body) under certain actuating voltage was obtained to estimate how much the maximum actuating force and deflection were. For the free body of bulge-diaphragm, the curve named *diaphragm characteristic curve* for the central deflection in proportion to action force was obtained for two cases of diaphragm thickness. Putting both kinds of curves (i.e. *piezoelectric characteristic curve* and *diaphragm characteristic curve*) together and with the condition of equal central deflections, the actuated central deflection was obtained under certain actuating voltage. Furthermore, it was observed that the volume displacement is in proportion to central deflection and the relation was obtained in both analytical and numerical analysis.

Besides free-body analysis, the whole model analysis of actuating module, as the Fig.4 shown, coupling piezoelectric actuator and bulge-diaphragm together, was treated numerically by ANSYS. Again, the linear relation of the diaphragm central deflection versus volume displacement corresponding to various actuating voltages was obtained.

3 Model and solution

3.1 Analytical model

As shown in Fig.3, the region inside the dash line is the analysis domain. The piezoelectric beam and bulge-diaphragm are separated and treated as free body for the analysis convenience. The shear mode piezoelectric

beam with two clamped edges boundary condition is subjected to interfacial reaction force on the bonded region. So its net deflection is the superposition of that induced by piezoelectric shear effect and reaction force in the static equilibrium state, and the approximate expression is formulated. Also, the bulge-diaphragm is modeled as a plate with two opposite clamped edges and two opposite simply supported edges. Neglecting the fluid pressure in the chamber, the bulge-diaphragm has only action force acting on the bonded surface of bulge, and its analytical deflection formula is obtained so the analytical volume displacement can be calculated. Fig.5 shows the analytical result of diaphragm deflection by MATLAB code for which the formula is obtained and stated below.

3.2 Analytical solution of the diaphragm

From the governing equation for the deflection of isotropic plate, shown as Eq.(1), and boundary condition, shown as Eq.(2), by Levy's method [Timoshenko et al. (1959)] we obtain the approximate analytical formula for the deflection of the diaphragm with uniformly distributed load, $q=F/uv$ over the bulge region, shown as Eq.(3). The seven constants in the formula are expressed by Eq.(3a) to Eq.(3g), in which the values of notations α_m and γ_m are calculated by Eq.(3h) and Eq.(3i).

3.3 Piezoelectric beam solution

As mentioned previously in analytical model, the free body of shear mode piezoelectric beam is modeled with two clamped edges and reaction force acting on the

bonded region. So, its net deflection, W_p , is obtained by superposing reaction force induced anti-deflection, W_f , and the electrically induced deflection, W_e . And, each approximate analytical solution are derived and showed in Eq.(4) to Eq.(6).

$$\frac{\partial^4 w}{\partial x^4} + 2 \frac{\partial^4 w}{\partial x^2 \partial y^2} + \frac{\partial^4 w}{\partial y^4} = \frac{q}{D} \quad (1)$$

$$\begin{aligned} \text{B. C. (i) } w = 0 \quad \text{(ii) } \frac{\partial w}{\partial x} = 0 \quad \text{for } x = \pm \frac{a}{2} \\ \text{(iii) } w = 0 \quad \text{(iv) } \frac{\partial^2 w}{\partial^2 x} = 0 \quad \text{for } y = 0 \quad \text{and } y = b \end{aligned} \quad (2)$$

$$w_d(x, y) = \begin{cases} \sum_{m=1,3,5,\dots} \left(K_m + A_m \cosh \frac{m\pi x}{b} + B_m \frac{m\pi x}{b} \sinh \frac{m\pi x}{b} \right) \sin \frac{m\pi y}{b} & \text{for } 0 \leq x \leq \frac{u}{2} \\ \sum_{m=1,3,5,\dots} \left(A'_m \cosh \frac{m\pi x}{b} + B'_m \frac{m\pi x}{b} \sinh \frac{m\pi x}{b} + C'_m \sinh \frac{m\pi x}{b} + D'_m \frac{m\pi x}{b} \cosh \frac{m\pi x}{b} \right) \sin \frac{m\pi y}{b} & \text{for } \frac{u}{2} \leq x \leq \frac{a}{2} \end{cases} \quad (3)$$

$$K_m = \frac{4Fb^4}{\pi^5 m^5 Duv} (-1)^{(m-1)/2} \sin \frac{m\pi v}{2b} \quad (3a)$$

$$A_m = \frac{K_m}{2\alpha_m + \sinh 2\alpha_m} \begin{bmatrix} -\gamma_m \cosh(2\alpha_m - 2\gamma_m) + (\gamma_m - 2\alpha_m) \cosh 2\gamma_m \\ -\sinh(2\alpha_m - 2\gamma_m) - (1 + 2\alpha_m^2 - 2\alpha_m \gamma_m) \sinh 2\gamma_m \end{bmatrix} \quad (3b)$$

$$B_m = \frac{K_m}{4\alpha_m + 2 \sinh 2\alpha_m} [(4\gamma_m - 2\alpha_m) \cosh 2\gamma_m - \sinh(2\alpha_m - 2\gamma_m) - 3 \sinh 2\gamma_m] \quad (3c)$$

$$A'_m = \frac{K_m}{4\alpha_m + 2 \sinh 2\alpha_m} \begin{bmatrix} -\gamma_m \cosh(2\alpha_m - 2\gamma_m) - \gamma_m \cosh(2\alpha_m + 2\gamma_m) \\ -\sinh(2\alpha_m - 2\gamma_m) + \sinh(2\alpha_m + 2\gamma_m) \\ + 2\gamma_m \cosh 2\gamma_m - (2 + 2\alpha_m^2) \sinh 2\gamma_m \end{bmatrix} \quad (3d)$$

$$B'_m = \frac{K_m}{8\alpha_m + 4 \sinh 2\alpha_m} [\sinh(2\alpha_m - 2\gamma_m) - \sinh(2\alpha_m + 2\gamma_m) - 8\gamma_m \cosh 2\gamma_m + 6 \sinh 2\gamma_m] \quad (3e)$$

$$C'_m = K_m [\gamma_m \cosh 2\gamma_m - \sinh 2\gamma_m] \quad (3f)$$

$$D'_m = \frac{K_m}{2} \sinh 2\gamma_m \quad (3g)$$

$$\alpha_m = \frac{m\pi a}{2b} \quad (3h)$$

$$\gamma_m = \frac{m\pi u}{4b} \quad (3i)$$

$$w_f(x) = \frac{1}{EI} \left\{ \begin{aligned} & \frac{F}{24 u_p} < x - (a - u_p)/2 >^4 \\ & - \frac{F}{24 u_p} < x - (a + u_p)/2 >^4 \\ & - \left[\frac{Fa}{12 u_p} - \frac{F}{6 u_p} (a - u_p)/2 \right] x^3 + \\ & \left[\frac{Fa^2}{24 u_p} - \frac{F}{4 u_p} (a - u_p)^2/4 + \frac{F}{6 u_p a} (a - u_p)^3/8 \right] x^2 \end{aligned} \right\} \quad (4)$$

$$w_e(x) = \begin{cases} d_{15} \frac{V}{t_p} \frac{a-u_p}{2} \frac{2x}{a-u_p} & \text{for } 0 \leq x \leq \frac{a-u_p}{2} \\ d_{15} \frac{V}{t_p} \frac{a-u_p}{2} & \text{for } \frac{a-u_p}{2} \leq x \leq \frac{a+u_p}{2} \\ d_{15} \frac{V}{t_p} \frac{a-u_p}{2} \frac{2(a-x)}{a-u_p} & \text{for } \frac{a+u_p}{2} \leq x \leq a \end{cases} \quad (5)$$

$$w_p(x) = w_e(x) + w_f(x) \quad (6)$$

3.4 Numerical model

In addition to analytical solution of free body, its corresponding numerical solution utilizing commercial finite element code, namely ANSYS, is obtained. The numerical analysis domain and boundary conditions is the same as that described in analytical model. The electrical-structure coupling element, say Solid5, is used to model the piezoelectric effect. All kinds of data extracted from analytical results are also obtained from the numerical results. Fig.3(b) shows the representative of finite element mesh and result for free-body numerical analysis. Besides the free-body analysis, the whole-model including piezoelectric beam actuator and bulge-diaphragm is created and coupled together numerically. And, the actuating deflection from the whole-model numerical results can be compared with that from the free-body analysis results. Fig.4(b) shows the representative of finite element mesh and result for whole-model numerical analysis.

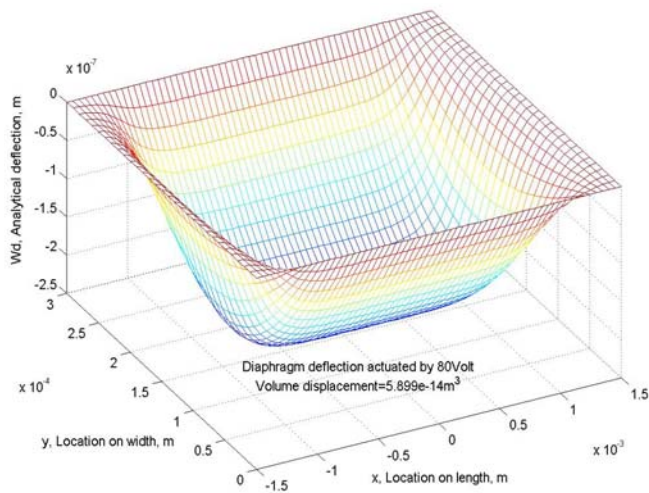


Figure 5 : Analytical result of diaphragm deflection

4 Results and discussions

Fig.6 shows both *diaphragm characteristic curves* and *piezoelectric characteristic curves*. The *piezoelectric characteristic curves* show the central deflection of the actuator decreasing with anti-deflection force (i.e. reaction force in free body) coming from the superposition of piezoelectric shear effect and reaction force. The deflection induced by piezoelectric shear effect mainly depends on shear piezoelectric coefficient, d_{15} , and the actuating voltage. And, the electrically induced deflection will be restrained by reaction force, so the deflection decreases with the increase of reaction force. In the figure, both analytical and numerical results are shown for comparison and they just appear a little difference in agreement. Thus, from these *piezoelectric characteristic curves*, we can obtain the maximum central deflection and estimate actuating force of shear mode piezoelectric actuator under certain actuating voltage. When the reaction force increases to some extent, it is also observed that the piezoelectric beam has buckling phenomenon, also shown in Fig.6.

For *diaphragm characteristic curves* showing action force dependent central deflection, there are two cases of curves corresponding to two thicknesses of $5\mu\text{m}$ and $10\mu\text{m}$ respectively. Both show a great agreement between numerical and analytical results. Combining *diaphragm characteristic curves* with *piezoelectric characteristic curves*, the intersection indicates the solution of actuated central deflection of the bulge-diaphragm

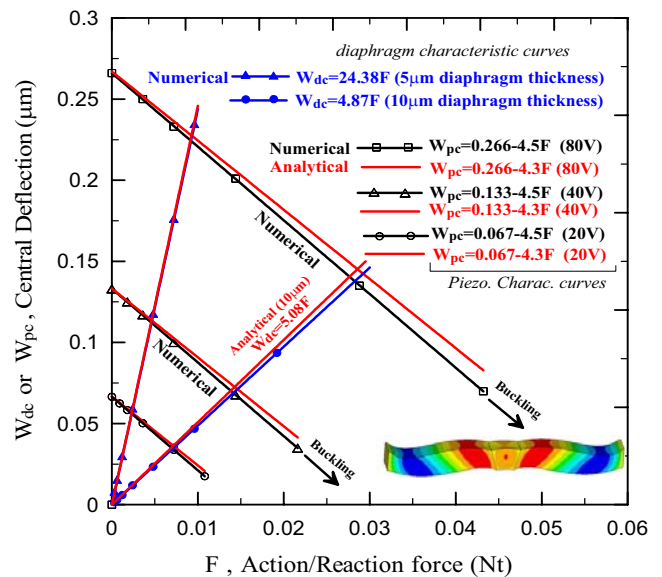


Figure 6 : Relation of central deflection versus action/reaction force in free-body analysis

and action/reaction force at the bonded interface in the equilibrium state under the certain couple of diaphragm thickness and actuating voltage. It is observed that the actuated central deflection of the bulge-diaphragm decreases with the increase of diaphragm thickness. Also, it is also observed that the actuated central deflection of the bulge-diaphragm approach to the central deflection of piezoelectric beam induced purely by piezoelectric shear effect as the diaphragm get thinner. In other words, as the diaphragm gets thinner, say $5\mu\text{m}$, the action/reaction force become smaller and the central deflection of piezoelectric actuator caused by piezoelectric shear effect dominates mostly the central deflection of the bulge-diaphragm.

Fig.7 shows the relation of actuated central deflection in proportion to actuating voltage for the bulge-diaphragm, where the data for fitting the solid curves are extracted from the intersections of *piezoelectric characteristic curves* and *diaphragm characteristic curves* shown in fig.6 by free-body numerical and analytical analysis; while the data for fitting dash lines are extracted from whole-model numerical analysis. It is observed that the numerical and analytical result in free-body analysis coincide very well except for a little discrepancy of the $10\mu\text{m}$ case. Moreover, some difference exists for the comparison between free-body analysis and whole-

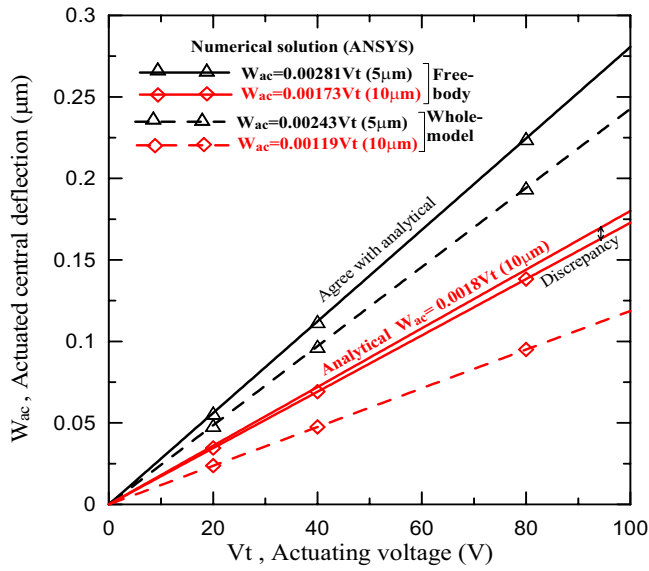


Figure 7 : Relation of actuated central deflection versus actuating voltage for diaphragm

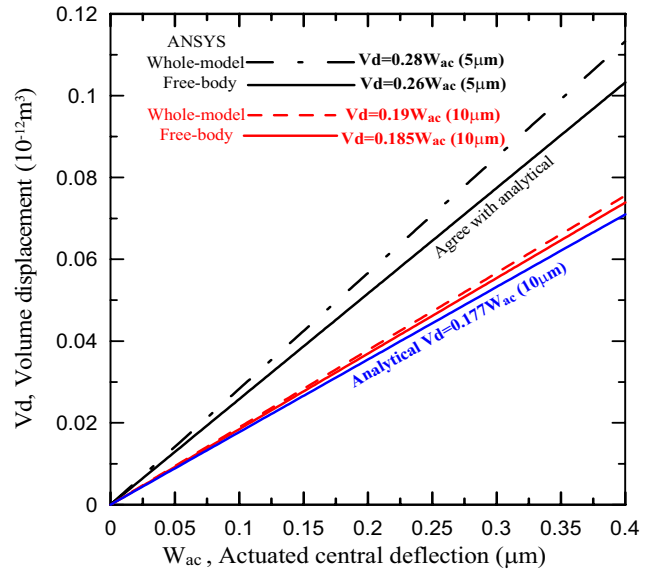


Figure 8 : Comparison of volume displacement in proportion to actuated central deflection between free-body and whole- model numerical analysis

model numerical analysis. It can be explained that the rigidity of model in free-body analysis is reduced comparing with that in whole-model analysis. Fig.8 shows the relation of volume displacement in proportion to actuated central deflection of the bulge-diaphragm. The solid curves are obtained from free-body numerical or analytical analysis while the dash curves come from whole- model numerical analysis. And, the curve-fitting function is also shown in the figure. Together with the fitting function shown in Fig.7, the volume displacement in proportion to actuating voltage can be calculated. Taking diaphragm thickness of $5\mu\text{m}$ for example, one have the relation of $V_d = 0.00068 V_t$ by whole-model numerical analysis so that the volume displacement is expected to be $5.44 \times 10^{-14} \text{m}^3$ under actuating voltage of 80volt. For the droplet with $40\mu\text{m}$ in diameter, this volume displacement of pressure chamber is supposed to be enough to eject it from the orifice.

5 Conclusion

1. A novel design of shear mode piezoelectric actuating module used for microdroplet ejector or inkjet printhead is proposed. Through numerical and analytical analysis, it is believed that the design could eject microdroplet of $40\mu\text{m}$ in diameter.

2. The *piezoelectric characteristic curve* for shear mode piezoelectric actuator, showing the central deflection decreasing with anti-deflection force under certain actuating voltage, was obtained to estimate how much the maximum actuating force and deflection were.
3. Both linear relations including diaphragm central deflection in proportion to actuating voltage and volume displacement in proportion to diaphragm central deflection are obtained.
4. Through the analysis, the diaphragm deflection and resulting swept volume change was predicted under certain actuating voltage. And, the effect of diaphragm thickness on chamber volume change was studied in this work.
5. All results obtained by analytical analysis are compared with those obtained by ANSYS numerical analysis, appearing well agreement.

Acknowledgement: This work was financially supported by the national science council under grant NSC 91-2218-E-212-002, which is gratefully acknowledged.

References

- Brumahl, J.; Grishin, A. M.** (2002): Piezoelectric Shear Mode Drop-On-Demand inkjet actuator. *Sensors and Actuators A*, Vol.101, pp.371-382.
- Edwards, C.; Albertalli, D.** (2001): Application of polymer LED materials using piezo ink-jet printing. In: *SID International Symposium Digest of Technical Papers*, pp. 1049-1051.
- Haynes, D. J.; Grove, M. E.; Cox, W. R.** (1999): Development and application by ink-jet printing of advanced packaging materials. In: *Proc. Int. Symp. on Advanced Packaging Materials*, pp.88-93.
- Hebner, T. R.; Wu, C. C.; Marcy, D.; Lu, M. H.; Sturm, J. C.** (1998): Ink-jet printing of doped polymers for organic light emitting devices. *Appl. Phys. Lett.*, Vol. 72 no.5, pp.519.
- Keefe, B. J.; Ho, M. F.; Courian, K. J.; Steinfield, S. W.; Chiders, W. D.; Tappon, E. R.; Trucba, K. E.; Chapman, T. I.; Knight, W. R.; Mortz, J. G.** (1994): Inkjet printhead architecture for high speed and high resolution printing. *U. S. Pat. 5648805*.
- Luginbuhl, P.** (1999): micromachined injector for DNA spectrometry. In: *Proc. IEEE Transducer '99*, Sendai, Japan, pp. 1130-1133.
- Perçin, G.; Khuri-Yakub, B.** (2003): Photoresist deposition without spinning. *IEEE transactions on semiconductor manufacturing*, Vol.16 no.3, pp. 452-459.
- Sakai, S.; Kobayashi, A.; Naka, T.; Yonekubo, S.; Mitsuzawa, T.; Shinada, S.** (1993): Inkjet Recording Head. *European Pat. 0573055A2*.
- Sweet, R. G.** (1971): Fluid Droplet Recorder. *U.S. Pat. 3576275*.
- Teng, K. F.; Vest, R.W.** (1998): Metallization of solar cells with ink jet printing and silver Metallo-Organic inks. *IEEE Trans. Components, Hybrids, and Manuf. Technol.*, Vol.11 no.3, pp. 291-297.
- Timoshenko, S.; Woinowsky-Krieger, S.** (1959): Rectangular plates with various edge conditions. In: second edition *Theory of Plates and Shells*, McGraw-Hill, New York.
- Yang, Y.; Chang, S. C.; Bharathan, J.; Liu, J.** (2000): Organic/polymeric electroluminescent devices processed by hybrid ink-jet printing. *J. Mater.Sci.:Mater. Electron.*, Vol. 11, pp.89-96.
- Zhang, T. Y.** (2004): Dielectric Breakdown Model For An Electrically Impermeable Crack In A Piezoelectric Material. *CMC: Computers, Materials & Continua*, Vol. 1, No. 1, pp. 107-116.